Photodissociation Dynamics of *tert*-Butyl Hydroperoxide at 193 nm

Seung Keun Shin and Hong Lae Kim*,†

Department of Chemistry, Kangwon National University, Chuncheon 200-701, Korea

Chan Ryang Park

Department of Chemistry, College of Natural Sciences, Kookmin University, Seoul, 136-702, Korea

Received: January 22, 1999; In Final Form: March 19, 1999

The photodissociation dynamics of *tert*-butyl hydroperoxide at 193 nm was investigated by measuring rotationally resolved laser-induced fluorescence spectra of OH fragments. The OH fragments are exclusively produced in the $X(^2\Pi_{1/2,3/2})$ state. From the spectra, the fraction of the available energy distributed among the products was found to be $f_r(OH) = 0.04$, $f_t = 0.56$, $f_{int}(t\text{-BuO}) = 0.40$, with negligible fraction of OH being in excited vibrational states. In addition, vector correlations were obtained by analyzing the Doppler profiles of the spectra. The detailed dynamics of the dissociation process is discussed compared to the dissociation of H_2O_2.

Introduction

Studies of molecular photodissociation dynamics are of fundamental importance to investigate electronic structures of molecules because the process is governed by the excited state and potential energy surfaces along the reaction coordinate. The detailed dynamics of the process can be understood by measuring energies and certain vector properties of the system. These physical properties of the system can be precisely measured from optical spectra in favorable cases where the photofragments absorb and/or emit radiation in an easily accessible spectral region. The Doppler-broadened absorption or emission spectra of the photofragments by polarized photolysis and probe light provide information on the energy distribution among various degrees of freedom of the fragments as well as directions of the transition dipole moment, recoil velocity, and angular momenta of the fragments.[1−3] From the measurements, the excited state and the potential energy surfaces along the reaction coordinate can be identified.

Spectroscopic transitions in molecules to the repulsive part of the potential energy surface result in continuous spectra. One can theoretically determine the energies of the excited states and describe the nature of the transitions by ab initio calculations. When the dissociation starts from a part of the repulsive potential surface, the angular distribution of the fragments is especially important among many experimental observables in determining the nature of the excited state. Maximum absorption of the dissociating light by the molecule takes place when the transition dipole moment of the molecule lies along the electric vector of the linearly polarized dissociating light. Thus, the angular distribution of the recoiling fragments measured relative to the electric vector of the dissociating light in the laboratory frame reveals the direction of the transition dipole moment of the molecule in the molecular frame. From the direction of the transition dipole moment, the symmetry of the excited state can be identified according to proper selection rules.

The Doppler profiles in polarized absorption and emission spectra of molecules have been thoroughly analyzed by Herschbach and Zare.[4,5] The line shapes of the spectra are determined by the coupling of rotational and translational motion of the molecules. Thus, the Doppler-broadened spectra of the photofragments provide relationships between the velocities and the rotational angular momenta of the fragments. The Doppler spectroscopic technique is limited by the resolution of the spectra. The translational energies of the fragments should be large enough to provide broad spectroscopic transitions, while the individual rotational transition should also be resolved in the spectra under the given resolution. A commercial dye laser currently available typically provides 0.04 cm^{-1} bandwidth in the visible region, and various laser spectroscopic techniques such as laser-induced fluorescence (LIF) have been widely used to obtain the high-resolution spectra of the photofragments.

Studies of the photodissociation of organic peroxides by irradiation of UV light have been reported for many years. In particular, the photodissociation of H_2O_2 in the first UV absorption band has been thoroughly studied.[6−8] The transition is assigned as $\sigma^* \leftarrow$ n whose transition dipole moment lies perpendicular to the O−O bond axis. The complete vector correlations have been measured, from which the detailed dynamics of the dissociation process at 266 nm have been analyzed. The photodissociation of $(CH_3)_3COOH$ is another good example of studying the dynamics by applying the Doppler spectroscopic technique. In addition, it is interesting to study the effect of alkyl substitution in H_2O_2 on the dissociation dynamics because the symmetry is lower and the substituted group is relatively heavy. $(CH_3)_3COOH$ is dissociated into *tert*-butoxy and OH radicals upon irradiation of the UV light. The photodissociation at 248 nm was studied by Simons and coworkers in which slightly negative $\mu-v$ ($\beta = -0.2$) and slightly positive $v-J$ correlation at high J have been observed.[9] In the case of H_2O_2 at 266 nm, a negative $\mu-v$ correlation ($\beta = -1$) was reported.[6] The perpendicular transition in this spectral region results in the negative limiting value of the $\mu-v$ correlation in H_2O_2 but the relatively large *t*-BuO group affects the dynamics of the dissociation resulting in the smaller translational anisotropy parameter β in the case of $(CH_3)_3COOH$. At 193 nm, it has been found that the transition leads to a mixture of the A

† E-mail: HLKIM@CC.KANGWON.AC.KR.

10.1021/jp990272s CCC: $18.00
Published on Web 05/06/1999

and B states in H_2O_2 and the dynamics has been studied by measuring the vector correlations of the OH fragments.[7,8] The dissociation directly occurs from the repulsive A and B states and most of the available energy has been found to be distributed in the product translation (~90%). Crim and co-workers have studied the vibration-mediated photodissociation via the fifth overtone excitation of the OH stretching vibration of $(CH_3)_3$-COOH.[10] They found large internal excitation in the *t*-BuO group contrary to the direct dissociation from the repulsive state. Thus, it is also interesting to study the photodissociation dynamics of this molecule at higher photon energies by examining the substituent effect on energy disposal and the vector correlations.

The dissociation dynamics has been studied by measuring the laser-induced fluorescence spectra of the OH fragments. By analyzing the Doppler profiles of the spectra the energy distribution and the vector correlations of the fragments have been obtained.

Experiment

The experiment was performed in a flow cell with a conventional pump−probe geometry. The cell is a cube made of stainless steel with four arms in which baffles are placed to minimize scattered light. The cell was evacuated at a pressure of about 10^{-3} Torr and the gaseous sample was continuously flowed at a sample pressure of about 20 mTorr. The *tert*-butyl hydroperoxide, purchased from Aldrich (90% purity), was pumped through a glass sample cell for at least 4 h until it reached a concentration of more than 95% before use.

The 193 nm dissociating light was obtained from an ArF excimer laser (Lambda Physik Lextra 50) whose output was linearly polarized with a stack of quartz plates at a Brewster angle. The horizontally polarized probe light is a frequency-doubled output of a dye laser (Lumonics HD-500) pumped by the second harmonic of an Nd:YAG laser (Lumonics YM-800). The two laser beams are temporally separated by about 30 ns. The 30 ns delay time between the pump and probe light and 20 mTorr sample pressure should ensure a nascent product energy distribution. The laser-induced fluorescence (LIF) spectra of the OH fragments were measured employing the A−X transition in UV. The 0−0 transition of OH was excited and the resulting total fluorescence was probed through a cutoff filter at 300 nm. The power of the probe laser light was kept as low as possible (typically 20 μJ/pulse) to avoid saturation and to minimize the scattered radiation. The scattered radiation was also cut off through baffles which are placed in the arms attached to the cell. In order to measure the Doppler profiles of the spectra, several rotational transitions were probed under high resolution. The bandwidth of the probe laser light is 0.06 cm^{-1} in the visible that is measured by the linewidth of the rotationally resolved gaseous I_2 spectra at ambient temperature. The horizontally polarized dissociating and probe laser beams are collinearly counterpropagated or introduced at a right angle to the cell to obtain two different experimental geometries. The former geometry provides $\epsilon_d \perp k_p$ and $\epsilon_d \parallel \epsilon_p$ while the latter provides $\epsilon_d \parallel k_p$ and $\epsilon_d \perp \epsilon_p$ where ϵ_d and ϵ_p are the directions of the electric vectors of the dissociating and probe lights and k_p is the propagation direction of the probe light, respectively.

The laser-induced fluorescence is detected through a collection lens by a PMT (Hamamatsu R212UH) whose direction of view is at a right angle to the two laser beams, and the detected signal is fed to a boxcar averager. The powers of the dissociating and the probe lights are separately measured and the detected signal is corrected for variation of the laser powers. A signal processor digitizes the signal that is stored and processed in a PC.

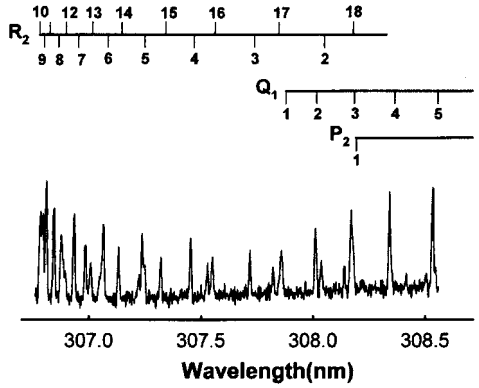

Figure 1. 1: A portion of the LIF excitation spectrum of OH produced from the photodissociation of *tert*-butyl hydroperoxide at 193 nm employing the 0−0, A ← X transition. The assignments are from ref 11.

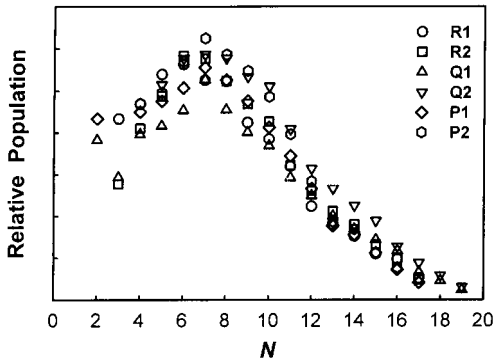

Figure 2. 2: Rotational population distribution of OH obtained from the LIF spectrum in Figure 1.

Results and Analyses

A portion of the LIF spectra of the OH fragments produced from the photodissociation of $(CH_3)_3COOH$ is presented in Figure 1. In the spectra, individual rotational transitions in the 0−0 band of the A−X transition are resolved and assigned according to Dieke and Crosswhite.[11] The OH spin−orbit population ratio was measured as a function of N. It was statistical and no preference in the population between the two spin−orbit states was found. The rotational population distribution which peaks at the rotational quantum number, $N = 7,8$ and extends to $N = 19$ is obtained from the measured spectra by using the reported Einstein B coefficients (Figure 2).[12] From the distribution, the average rotational energy of OH was found to be about 1600 cm^{-1}. The rotational transitions from the 1−1 band region have been measured but no appreciable intensities exceeded the noise in the spectra. The rotational transitions from the higher vibrational states of OH could not be measured from diagonal transitions such as 2−2 and 3−3 bands due to extensive predissociation from the higher vibrational states in the A state. However, since no appreciable slow speed components corresponding to the higher vibrational states of OH have been observed in the Doppler profiles, it was concluded that the population of OH in the higher vibrational states is negligible.

Correlations of rotation with translational motion have been thoroughly analyzed by Dixon[13] and the anisotropy is defined by a number of bipolar moments of the translational and

rotational angular distributions. The Doppler-broadened line shape in the LIF spectra of the photofragments depends on the rotational alignment, the polarizations of the photolysis and probe lights, the excitation−detection geometries, and the rotational branch transitions probed. The generalized line shape functions are then given by

$$g(\chi_D) = \frac{1}{2\nu_D}[g_0 + g_2P_2(\chi_D) + g_4P_4(\chi_D) + g_6P_6(\chi_D)]$$

where χ_D and ν_D are the relative and the maximum Doppler shift, respectively, and P's are the even-order Legendre polynomials. The Legendre polynomials of the fourth and sixth order are often neglected since the contribution of these high order terms to the Doppler profiles are small compared to the experimental errors. The multiplier, g's in the above equation, are the linear combination of the bipolar moments, β_0^k, which are given by

$$g_0 = b_0 + b_1\beta_0^2(02)$$

$$g_2 = b_2\beta_0^2(20) + b_3\beta_0^0(22) + b_4\beta_0^2(22)$$

where b's can be calculated from the excitation−detection geometries and the angular momentum coupling factors defined by Dixon. In this experiment, the two different excitation−detection geometries described in the Experimental Section have been employed, and the corresponding b values have been obtained for the different rotational branch transitions.[14] The bipolar moments, $\beta_0^2(02)$, $\beta_0^2(20)$, $\beta_0^0(22)$, $\beta_0^2(22)$ represent the rotational alignment, $\beta_{\mu J}$, translational anisotropy, $\beta_{\mu\nu}$ (=2 $\beta_0^2(20)$), $\nu-J$, and $\mu-\nu-J$ photofragment vector correlations, respectively. The experimental Doppler profiles are fitted by the equation

$$g(\chi_D) = (1/2\nu_D)[1 + \beta_{eff}P_2(\theta)P_2(\chi_D)]$$

where θ is the angle between the recoil velocity and the probe direction and

$$\beta_{eff} = [b_2\beta_0^2(20) + b_3\beta_0^0(22) + b_4\beta_0^2(22)]/g_0P_2(\theta)$$

From the least-squares fit of the observed profiles by the above equation, the four bipolar moments can be calculated by solving the linear equations.

The Doppler resolved spectra have been measured for the P_1 and Q_1 or R_1 and Q_1 rotational branch transitions for the rotational quantum numbers $N = 4$, 5, 6, 9, 10, 13, 14, 15, and 17 which are well separated from other transitions. In Figure 3, typical Doppler-broadened LIF spectra for $N = 13$ are presented. Since the *t*-BuO fragments should have internal energy distributions, the OH fragments should have corresponding speed distributions. However, the internal energy distributions of the *t*-BuO fragments have not been measured in this experiment. Thus, the measured profiles have been fitted assuming Gaussian speed distribution with various widths. In order to find the best fits, the following procedures were employed. First, the best fit was found to the observed profile of one rotational branch transition varying β_{eff}, the average speed, and the width of the speed distribution. The measured average speed and the width for the best fit are 4600 and 1200 m/s for $N = 13$, respectively. Then, for the profiles of the different rotational branch transitions under different experimental geometries at the same N, the best fit was obtained by just varying β_{eff}. From the measured β_{eff}'s for the same N, the bipolar moments are calculated by solving the linear equations. The calculated bipolar moments for different N's are presented in Figure 4. In the figure, the negative translational anisotropy($\beta_{\mu\nu} = -0.2$) indicates the OH fragments should be essentially ejected perpendicular to the transition dipole moment of the parent molecule, although the value is far from the limiting value of −1. The positive increasing $\nu-J$ correlation with increasing N implies more parallel orientation of the rotational angular momentum J_{OH} to the recoil velocity ν_{OH} (out-of-plane dissociation). In addition, slightly positive $\mu-\nu$ and positive $\mu-\nu-J$ correlations were also observed.

In Figure 5, the Λ-doublet distribution in the OH fragment is presented as a function of N while the statistical ratio is unity. The measured distribution shows that the Π^- Λ-doublet state is preferentially populated at high N, which suggests that the OH fragments tend to rotate in the plane perpendicular to the dissociating bond axis.

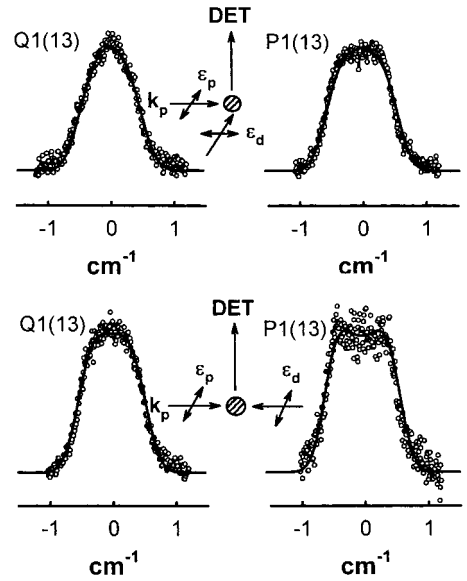

Figure 3. 3: Doppler profiles of the rotationally resolved spectra of OH at the rotational quantum number 13 under two different experimental geometries described in the Experimental Section. Smoothe curves are the best fits to the equation given in the text.

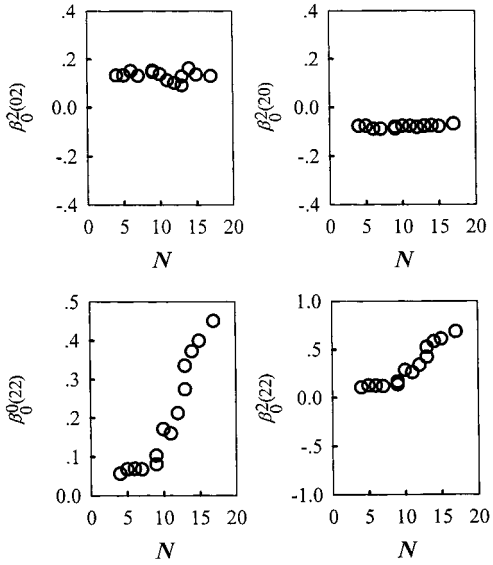

Figure 4. 4: Vector correlations as a function of the rotational quantum numbers by solving the linear equations (see the text).

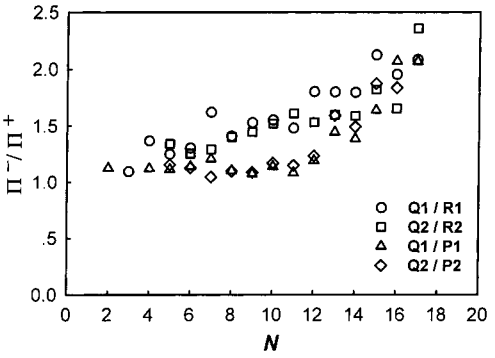

Figure 5. 5: Λ-doublet distribution of OH as a function of the rotational quantum numbers from the measured LIF spectra in Figure 1.

Discussions

The absorption spectrum of *tert*-butyl hydroperoxide in UV is qualitatively similar to that of H_2O_2.[15] The absorption starts from around 300 nm and continuously increases to the shorter wavelength. In H_2O_2, the excited states responsible for the absorption in these wavelengths are the A ^{1}A, B ^{1}B, and C ^{1}A states which are all repulsive and correlated to the two ground electronic state OH fragments. The transition dipole moments of the absorption from the ground X ^{1}A state to the ^{1}A state are parallel to the C_2 axis (perpendicular to the O−O bond) while the transition dipole moment to the ^{1}B state is perpendicular to the C_2 axis. An ab initio calculation predicts that the angle between the internuclear axis and the transition dipole moment to the ^{1}B state is 20°.[16] Assuming instantaneous dissociation upon absorption, translational anisotropy parameters of −1 and 1.6 would be expected for the X → A and X → B transitions, respectively. Based upon the translational anisotropy measurement, the absorption at 193 nm is assigned as a transition to a mixture of 60% of the A state and 40% of the B state.[8] Although the *tert*-butyl substitution in H_2O_2 lowers the symmetry, a qualitative trend of the similar n → σ^* transition at these wavelengths can be assumed in *tert*-butyl hydroperoxide. In this case, the translational anisotropy parameter would be expected to be close to zero. The measured translational anisotropy parameter of −0.2 in this experiment shows the perpendicular nature of the transition at 193 nm but is much larger than the limiting value, −1 for the pure perpendicular transition. The deviation might be in part caused by a lifetime of the parent molecule comparable or longer than a single rotational period. However, judging from the impulsive nature of the dissociation which will be discussed later and the longer rotational period due to heavy *tert*-butyl substitution compared to H_2O_2, slow dissociation is unlikely. It is rather reasonable to believe that the large deviation of the anisotropy parameter is caused by the mixed character of the transition, perpendicular and parallel. Another explanation would be dynamical nature of the dissociation as mentioned by Simons et al. in the photodissociation at 248 nm.[9] The bending torque would deflect the OH fragment away from the recoil axis and hence reduce the $\mu-\upsilon$ correlation. The possibility of a mixed transition was excluded in the photodissociation at the longer wavelengths because the excitation energy is lower. In this experiment, however, the large deviation of the anisotropy parameter may be due to the mixed transition and/or to the dynamical nature of the dissociation as well. The contribution of each transition at this wavelength could be estimated if accurate excited state potential energy surfaces would be available.

TABLE 1: Fraction of the Available Energy Distributed among the Products Produced from the Photodissociation of $(CH_3)_3COOH$

E_{av} (cm^{-1})	$\langle f_t \rangle$	$\langle f_t(OH) \rangle$	$\langle f_v(OH) \rangle$	$\langle f_{int}((CH_3)_3CO) \rangle$
39 150[a] (at 193 nm)	0.56	0.04	<0.01[b]	0.4
impulsive model	0.58	0.029	0.001	

[a] $E_{av} = h\nu + E_{int}((CH_3)_3COOH$ at 300 K) − $D_0((CH_3)_3COOH)$. [b] Approximated from the noise in the spectra.

The available energy which can be distributed among the fragments is 39 150 cm^{-1}. The measured fractions of the available energy are listed in Table 1. The measured energy partitioning in the fragments is well explained by the impulsive dissociation model which assumes direct and fast dissociation.[17] In the model, the initial excitation turns on the impulsive force between the departing O−O atoms. The linear momentum of the atoms is then transferred to the fragments and the average translational and internal energies of the fragments are calculated based upon the momentum and energy conservation. The measured energy distribution implies the dissociation is direct and fast from the repulsive surfaces as expected. However, a recent quantum dynamical calculation of the photodissociation of H_2O_2 shows the rotational population distribution of the OH fragment should be Gaussian-like with a tail at high *N* due to bending and torsional couplings.[18,19] If more torsional couplings are taken into account, the distribution shows more tailing to the high *N* side. The ab initio calculations of the equilibrium geometry of H_2O_2 indicate the dihedral angle of 120° at the trans planar geometry and the barrier for corresponding cis−trans configurational change is 386 cm^{-1}.[20] The alkyl substitution slightly opens the dihedral angle in CH_3COOH and greatly reduces the barrier (∼80 cm^{-1}). Assuming the similar trend in *tert*-butyl substitution in *tert*-butyl hydroperoxide, the barrier is expected to be much lower than the zero-point energy of the OH torsional motion. Thus, the wide angle torsional motion of the parent molecule is likely transformed to the fragment OH rotational motion upon dissociation and the rotational population distribution observed in this experiment reflects the importance of the parent torsional motion, especially at high N. The fact that the parent torsional motion should play an important role in the OH fragment rotation is ascertained by the $\upsilon-J$ vector correlation measured in this experiment.

Coupling between rotation and translational motion can be analyzed by the shape of the Doppler profiles of the spectra of the OH fragment. Since the $\upsilon-$J correlation is developed at the moment of dissociation, it can be observed even in the isotropic dissociation. If the source of the fragment OH rotation is the bending torque or the impulsive force, the rotational angular momentum should be aligned perpendicular to the recoil direction. In this case, the negative $\upsilon-J$ correlation is expected. However, if the parent torsional motion is the source of the OH rotation, the rotational angular momentum should be aligned parallel to the recoil direction and hence the positive $\upsilon-J$ correlation would be observed. The $\upsilon-J$ correlation measured in this experiment is positive and increases as *N* increases, implying again that the parent torsional motion plays the important role in the fragment OH rotation.

In a diatomic molecule with a singly occupied p_π orbital such as OH produced in this experiment, coupling between the electronic angular momentum and nuclear rotation splits the two degenerate states of $\Lambda = \pm 1$, the orbital angular momentum projection to the internuclear axis.[21] In the limit of high rotation, the p_π orbital is approximated as a lobe aligned perpendicular to the plane of rotation (Π^-, the lower Λ state) or a lobe in the

plane of rotation (Π^+, the upper Λ state). According to the parity selection rule, the Π^- state is populated by the Q-branch rotational transition and the Π^+ state by the R- and P-branch transitions in the electronic transition. Thus, the specific Λ-doublet population can be experimentally measured in the spectra. The distribution between the two Λ-doublet states of OH produced in the photodissociation depends on the correlation on the p_π orbital of the OH fragment with the orbitals of the parent molecule and how the p_π orbital is generated upon dissociation, that is the mechanism of the dissociation process. In the photodissociation of H_2O_2 at 193 nm, a slight propensity in the Π^- state is observed ($\Pi^-/\Pi^+ = 1.4$).[7] The transition to the A and B states are the $n \rightarrow \sigma^*$ transitions which are expected to lead to the equal population between the two Λ-doublets unless there is any dynamical effect. However, the measured unequal population distribution is explained by the nonnegligible $nn \rightarrow \sigma^*\sigma^*$ electronic configuration mixed into the wave function at large O−O distance, which leads to $\Pi^-/\Pi^+ > 1$. The measured Λ-doublet distribution in this experiment shows a propensity in the Π^- state and the propensity is increased as N is increased, indicating the unpaired p_π orbital of the OH fragment is more aligned perpendicular to the plane of rotation. A similar argument can be applied to the present study. In the dissociation of *tert*-butyl hydroperoxide, the configuration interaction as in H_2O_2 is even more probable because of the low symmetry leading to $\Pi^-/\Pi^+ > 1$. In addition, the higher propensity in the Π^- state of OH recoiling with higher rotational angular momentum indicates that the p_π orbital lobe of the OH fragment conserves some of the orientations of the corresponding p_π orbital in the excited parent molecule just before dissociation and reflects the importance of the angular motion such as torsion on the excited surfaces.

In summary, the photodissociation of *tert*-butyl hydroperoxide at 193 nm takes place fast and directly from the repulsive surfaces. The energy disposal in the products can be accounted for by the impulsive dissociation model. It is found that the parent torsional motion plays an important role in the rotation of the OH fragment.

Acknowledgment. This work has been financially supported by Korea Science and Engineering Foundation and the Ministry of Education in Korea.

References and Notes

(1) Hall, G. E.; Houston, P. *Annu. Rev. Phys. Chem.* **1989**, *375*, 40.
(2) *Molecular Photodissociation Dynamics*; Ashfold, M. N. R., Baggott, J. E., Eds.; Royal Society of Chemistry: London, 1987.
(3) Simons, J. P.; *J. Phys. Chem.* **1987**, *91*, 5378.
(4) Zare, R. N.; Herschbach, D. R. *Proc. IEEE* **1963**, *51*, 173.
(5) Greene, C. H.; Zare, R. N. *Annu. Rev. Phys. Chem.* **1982**, *33*, 119.
(6) Gericke, K.-H.; Klee, S.; Comes, H. J.; Dixon, R. N. *J. Chem. Phys.* **1986**, *85*, 4463.
(7) Ondrey, G.; van Veen, N.; Bersohn, R. *J. Chem. Phys.* **1983**, *78*, 3732.
(8) Grunewald, A. U.; Gericke, K.-H.; Comes, H. J. *J. Chem. Phys.* **1987**, *87*, 5709.
(9) August, J.; Brouard, M.; Docker, M. P.; Milne, C. J.; Simons, J. P.; Lavi, R.; Rosenwaks, S.; Schwartz-Lavi, D. *J. Phys. Chem.* **1988**, *92*, 5485.
(10) Likar, M. D.; Baggott, J. E.; Sinha, A.; Ticich, T. M.; Vander Wal, R. L.; Crim, F. F. *J. Chem. Soc., Faraday Trans.* **1988**, *84*, 1483.
(11) Dieke, G. H.; Crosswhite, H. M. *J. Quant. Spectrosc. Radiat. Transfer* **1962**, *2*, 97.
(12) Chidsey, I. L.; Crosely, D. R. *J. Quant. Spectrosc. Radiat. Transfer* **1980**, *23*, 187.
(13) Dixon, R. N. *J. Chem. Phys.* **1986**, *85*, 1866.
(14) Baek, S. J.; Park, C. R.; Kim, H. L. *J. Photochem. Photobiol. A* **1997**, *104*, 13.
(15) Baulch, D. L.; Cox, R. A.; Hampson Jr, R. F.; Kerr, J. A.; Troe, J.; Watson, R. T. *J. Phys. Chem. Ref. Data* **1984**, *13*, 1259.
(16) Chevaldonnet, C.; Cardy, H.; Dargelos, A. *Chem. Phys.* **1986**, *102*, 55.
(17) Tuck, A. F. *J. Chem. Soc., Faraday Trans. 2* **1977**, *73*, 689.
(18) Bersohn, R.; Shapiro, M. *J. Chem. Phys.* **1986**, *85*, 1396.
(19) Zhang, D. H.; Zhang, J. Z. H. *J. Chem. Phys.* **1992**, *98*, 6276.
(20) Bair, R. A.; Goddard III, W. A. *J. Am. Chem. Soc.* **1982**, *104*, 2719.
(21) Hanazaki, I. *Chem. Phys. Lett.* **1993**, *201*, 301.